

SALTON SEA GEOTHERMAL RESERVOIR SIMULATIONS*

T. D. Riney, J. W. Pritchett and S. K. Garg

Systems, Science and Software
P. O. Box 1620, La Jolla, California 92038

The Salton Sea Geothermal Field (SSGF) is a high salinity, high-temperature resource. The San Diego Gas & Electric Company has constructed a nominal 10 MWe Geothermal Loop Experimental Facility (GLEF) which will use brine produced from Magma Power Company's Woolsey No. 1 (W1) and Magmamax No. 1 (M1) wells; the Magmamax No. 2 and No. 3 (M3) wells will be used for reinjection. Intermittant brine production/injection has been performed since May 1976, but no associated fluid flow data have been published. The Lawrence Livermore Laboratory (LLL), however, has correlated the data available from surface measurements and logs from various wells in the SSGF. We have used this limited data base and the MUSHRM simulator to synthesize a preproduction reservoir model for a portion of the SSGF which contains the GLEF site. The simulator is then applied to the model to examine reservoir performance under different assumptions to improve our understanding of the system and its potential for exploitation.

The main sequence reservoir rock in the SSGF is bedded sandstone with shale lenses and layers, overlain with a relatively impermeable shale bed (cap-rock), and is believed by the LLL investigators to be separated into "upper" and "lower" reservoirs by a relatively thick and continuous shale layer [Towse, 1975; Schroeder, 1976]. From studies of cores, cuttings and logs from wells drilled in the SSGF, Towse [1975] determined the approximate depths to the top of the upper reservoir and to the major shale break separating the upper and lower reservoirs. Since the geologic layers dip in a northwesterly direction essentially parallel to the Brawley Fault Zone, we selected the region covered by the finite difference mesh in Figure 1 for our study. A cross-section is constructed by projecting the data onto a vertical plane parallel to the surface trace of the Brawley Fault Zone (Figure 2). The interfaces between the geologic layers are taken to be planes dipping to the northwest which approximate the points depicted. The temperature-depth profiles measured in the geothermal wells [Palmer, 1975] have been projected to construct the approximate temperature contours shown in Figure 2. The GLEF production wells (W1, M1) are perforated almost entirely within the upper reservoir whereas the injection wells (M2, M3) are perforated mostly within the lower reservoir.

Whether or not the interfacial shale barrier prevents significant fluid exchange between two re-

servoirs will have a profound effect on their response to imposed production/injection conditions. In the absence of vertical permeability data, two limiting cases were analyzed.

1. Production from upper reservoir without injection, i.e., shale barrier prevents fluid injected into lower reservoir from entering upper reservoir.
2. Production and injection occur in upper reservoir, i.e., vertical fractures channel injected fluid into upper reservoir.

Schroeder [1976] analyzed the sparse data available from drillstem test records from M1 and W1 and concluded that the horizontal permeability of the reservoir sands in the upper reservoir shale/sand sequence exceeds 500 md. The sands comprise over 50 percent of the sequence and their porosity exceeds 0.3. For the upper reservoir sequence we assume the following properties: rock horizontal permeability = 500 md; grain density of rock = 2.65 g/cm³; initial porosity of rock = 0.20; rock thermal conductivity = 2.1×10^5 ergs/sec-cm-°C; rock specific heat = 10^7 ergs/g-°C; brine salinity(s) = 0.25; irreducible liquid saturation = 0.3 and irreducible vapor saturation = 0.05. The latter two parameters define the relative permeabilities, in the case of two-phase flow, using the Corey formulation.

The 2D areal version of S³'s MUSHRM reservoir simulator is capable of treating the dipping and thickening upper reservoir if we consider the component of gravity along the direction of dip and vary the rock properties to offset variations in thickness. The Brawley and Red Hill faults are assumed to prevent any fluid flow across the side boundaries (Figure 1). The fluids produced by wells on opposite sides of the Brawley Fault appear to have a different origin, but there is no definite evidence that the Red Hill fault is a sealing fault.

Figure 2 shows that the temperature at the mid-plane of the upper reservoir is much less at the southeastern end (left, $y=0$) than at the northwestern end (right, $y=L$). No pressure data are available. Using the S³ brine equation-of-state ($s=0.25$) and the temperature-depth profiles at the two ends, the corresponding mid-plane hydrostatic pressures are computed to be $P(0)=38.02$ bars and $P(L)=85.07$ bars. By considering the temperature variation and dip angle along the length of the reservoir (Figure 2), it is found that if there were no preproduction flow, the value of $P(L)$ would need to be 88.24 bars. The lengthwise pressure

*Work performed under NSF Grant No. AER75-14492 A01.

drive, $\Delta P = 3.17$ bars, apparently causes an influx of $\sim 50^\circ\text{C}$ groundwater from the southeast end ($y=0$) which would cool the upper reservoir if hot brine infusion from the lower reservoir were completely precluded by the shale barrier. A vertical permeability of 0.01 to 0.1 md would suffice for steady state convective transport across the shale barrier to swamp heat conduction, a value too small to affect reservoir response to exploitation.

These boundary conditions and reservoir properties were incorporated into MUSHRM and a series of calculations performed until a satisfactory match with the mid-plane preproduction temperatures in the upper reservoir was obtained. A 1D version was first applied to the dipping and thickening upper reservoir with the provision that for each zone there is infusion of 275°C brine ($s = 0.25$) at the rate required to obtain the corresponding projected mid-plane preproduction temperature. The total rates of 50°C groundwater ($s = 0.25$) influx and convective brine infusion are calculated to be $\dot{M}_0 = 26.7$ kg/sec and $\dot{M}_c = 294.8$ kg/sec, respectively. These totals and the lengthwise variation of the influx rate were maintained, but the temperature of the brine and the lateral distribution of the influx rate were allowed to vary in a subsequent series of 2D areal calculations. A symmetric distribution with maximum at the center was found to best fit the lateral variation of the mid-plane temperatures measured in the wells. Having selected the lateral distribution influx rate, the calculation was then rerun with the temperature of the brine source reduced to 251°C in order to better match the mid-plane temperatures. The desired mid-plane temperatures for the well locations are satisfactorily matched by the steady-state temperature contours calculated with the preproduction model (Figure 3). The velocity plot, Figure 4, shows that the infusion of hot brine from the lower reservoir pushes a large part of the incoming cold groundwater to the edges of the upper reservoir, producing the lower temperatures there.

We make the conservative assumption that the infusion of hot brine from the lower reservoir remains at its preproduction value ($\dot{M}_c = 294.8$ kg/sec) during exploitation of the upper reservoir. The hydrostatic pressure at the downstream end of the reservoir is maintained ($P(L) = 85.07$ bars); the production/injection rates are held constant during the course of a given calculation. When injection occurs, the injected brine is taken to be 50°C and to comprise 80 percent of the mass produced ($\dot{M}_I = 0.8 \dot{M}_p$).

A production rate of $\dot{M}_p = 100$ kg/sec is assumed appropriate for a net 10 MWe at the GLEF site. For convenience, this equivalence is used for higher rates, e.g., nominal 50 MWe means $\dot{M}_p = 500$ kg/sec. Since the temperature of the produced brine declines with time, these nominal values of electrical power production become less meaningful.

A series of preliminary calculations using an approximate equation-of-state was performed to examine the sensitivity to the boundary condition assumed at the upstream (southeast) end of the reservoir. Above nominal 50 MWe (production only) to 250 MWe (with injection), the assumption of constant hydrostatic pressure requires increasing ground-water influx above the preproduction value. Constant ground-water flow ($\dot{M}_0 = 26.7$ kg/sec.) was

selected as being a more realistic boundary condition since the available groundwater is limited primarily to leakage from irrigation canals supplied by the Colorado River.

Essentially steady-state pressure and velocity fields are soon established wherein the mass flow rate out of the downstream end of the reservoir (\dot{M}_L) plus the excess rate of production over injection must balance the mass rate of fluid entering the reservoir from the upstream groundwater and convection mass sources: $\dot{M}_L + (\dot{M}_p - \dot{M}_I) = \dot{M}_0 + \dot{M}_c = 321.5$ kg/sec. The following table gives the values of \dot{M}_L for imposed production/injection rates of interest. For $\dot{M}_L < 0$, fluid is entering the downstream end of the upper reservoir and the time (t_r) required for this replacement fluid mass to equal the total preproduction fluid mass in the upper reservoir (3.05×10^{12} kg) is also given. Power production in excess of nominal 50 MWe (production only) to 250 MWe (with injection) requires a tremendous replenishment of hot brine from the downstream end.

PRODUCTION RATES		PRODUCTION ONLY ($\dot{M}_I = 0$)		WITH INJECTION ($\dot{M}_I = 0.8 \dot{M}_p$)	
NOMINAL MWe	\dot{M}_p (kg/sec)	\dot{M}_L (kg/sec)	t_r (YRS)	\dot{M}_L (kg/sec)	t_r (YRS)
0	0	322	---	322	---
10	100	222	---	302	---
50	500	-179	542	222	---
250	2500	-2179	44	-179	542
325	3250	-2929	33	-329	295

Two nominal 50 MWe simulations treated the four-zone production/injection pattern shown in Figure 1. All production wells are located within the two computational zones containing W1 and M1, and all injection wells are in the zones containing M3 and M2. Figure 5 shows the time history of the bottomhole temperature of the brine produced from each of the two production zones. Results for both assumptions regarding the effectiveness of the shale barrier are presented. The proximity of the production zones to the injection zones causes a rapid decline of the temperature of the produced fluid when the injected fluid is assumed to enter the upper reservoir. Without injection, there is a reversal of the flow at the downstream boundary as anticipated by the table.

From the preproduction model it is apparent that the preferred production region of the upper reservoir is near its center; the injection zones should be either along the two edges of the reservoir or downstream to minimize potential cooling of the produced brine. Figure 6 depicts an improved (and symmetric) production/injection pattern used for a nominal 50 MWe simulation. Both production and injection areas are five times those used above and the intensity of exploitation (well spacing) is more realistic. Figure 7 shows the time history of the bottomhole temperature of the produced brine averaged over all the calculational zones in the production area for the case where it is assumed that the injected fluid enters the upper reservoir. The maximum and minimum brine temperature decline of only 2°C over the 30-40 year period is in sharp contrast to the result obtained with the result obtained with the simple four-zone pattern with injection. Flow at the downstream end of the reservoir

remains outward, in agreement with the table; no assumption on the availability of hot brine recharge is required (with injection).

Two additional simulations examined the response of the upper reservoir to nominal 250 MWe power production using a preferred production/injection pattern (Figure 6). Compared to the nominal 50 MWe simulations, the intensity of exploitation is one-third that employed when using the simple four-zone pattern and five-thirds that employed when using the improved pattern. Figure 8 shows the time history of the maximum, minimum and average bottom hole temperature of produced fluid for the case where all of the injected fluid is assumed to enter the upper reservoir. A 20°C decline of the averaged temperature is predicted over a 30-40 year period. There is a reversal of the flow at the downstream end required for this large scale exploitation of the upper reservoir even with injection. The case where no injected fluid is assumed to enter the upper reservoir results in an average temperature decline of only 3°C over a 30-40 year period. Attainment of this reservoir response, however, requires tremendous replenishment of hot brine at the northwest end.

Because of the limited data base, the simulations presented necessarily invoked a variety of hypotheses concerning geology, temperature and pressure, groundwater flow, convective flow, etc. and will likely require revision to include new information as the SSGF resource moves from the exploration and assessment stage of development to the exploitation and utilization stage. Only the upper reservoir of a portion of the SSGF was treated. This portion of the resource appears capable of supplying brine for a net 50 MWe demonstration plant with very little temperature decline over a 30-40 year design life. Uncertainties regarding boundary conditions and the effectiveness of the shale barrier between the upper and lower reservoir prevent an evaluation of the ability of the upper SSGF to sustain a 250 MWe plant. The capacity of the lower reservoir should also be considered in such an evaluation.

REFERENCES

Palmer, T.D. [1975], "Characteristics of Geothermal Wells Located in the Salton Sea Geothermal Field, Imperial County, California," Lawrence Livermore Laboratory Report, UCRL-51976.

Schroeder, R.C. [1976], "Reservoir Engineering Report for the Magma-SDG&E Geothermal Experimental Site Near the Salton Sea, California," Lawrence Livermore Laboratory Report, UCRL-5094.

Towse, D.F. [1975], "An estimate of the Geothermal Energy Resource in the Salton Trough, California and Mexico," Lawrence Livermore Laboratory Report, UCRL-51851.

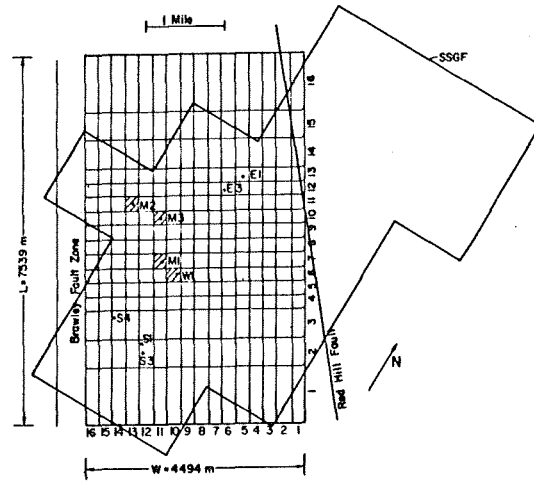


Figure 1. Portion of the SSGF chosen for simulation. Development wells within the region are also shown.

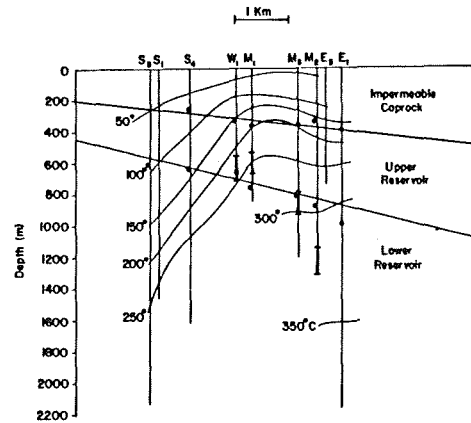


Figure 2. Vertical section and projected data from development wells. Points due to Towse [1975].

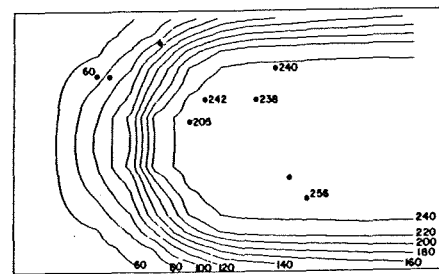


Figure 3. Preproduction model temperature contours (°C) compared with mid-plane temperatures measured at well locations.

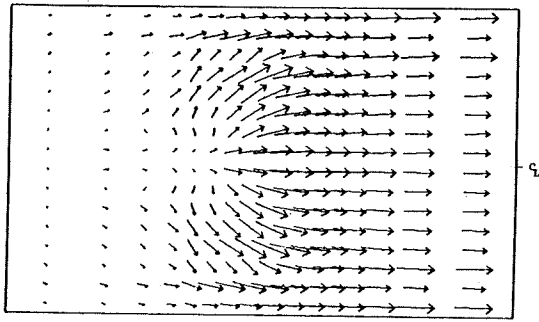


Figure 4. Preproduction model velocity field in upper reservoir (longest vector is 0.91×10^{-4} cm/sec).

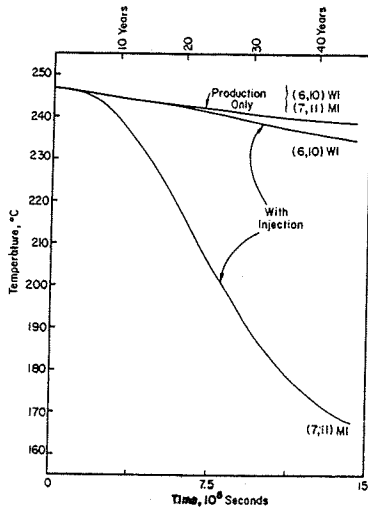


Figure 5. Wellbottom temperature of brine produced from upper reservoir (nominal 50 MWe, simple four zone pattern).

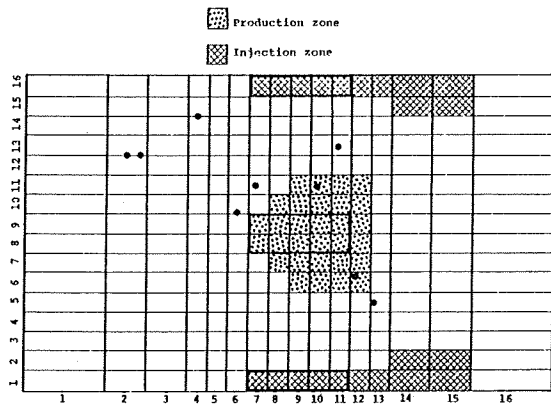


Figure 6. Improved production/injection patterns for exploitation of upper reservoir: nominal 50 MWe (heavily outlined areas) and nominal 250 MWe (total areas shown).

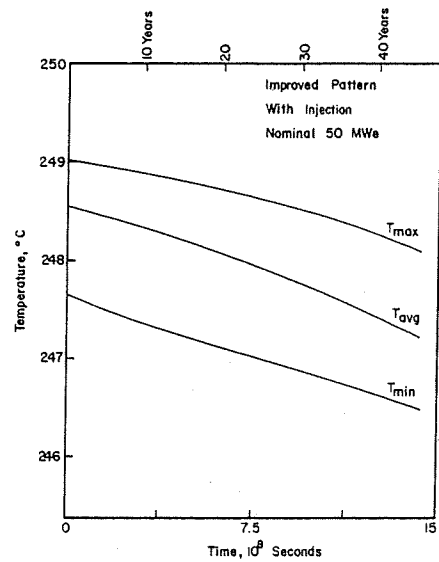


Figure 7. Wellbottom temperature range of brine produced from upper reservoir (nominal 50 MWe, improved pattern with injection).

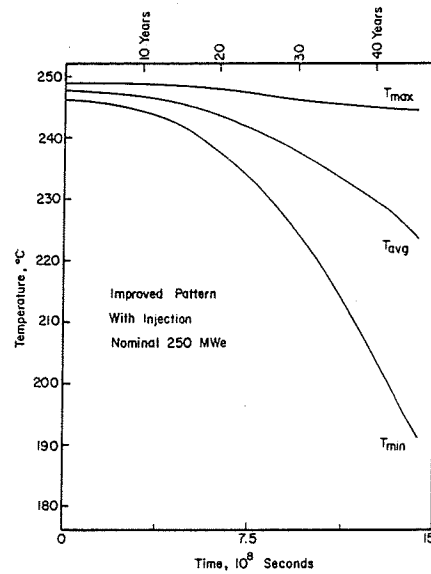


Figure 8. Wellbottom temperatures of brine produced from upper reservoir (nominal 250 MWe, improved pattern with injection).